Czech Technical University in Prague
Faculty of Civil Engineering
Department of Mechanics

Effect of geometry on homogenised properties of selected auxetic metamaterials

Nataša Jošková
Supervisor: *Ing. Martin Doškář, Ph.D.*

Soutěž o Cenu akademika Bažanta

Prague, April 2024

Acknowledgements

I would like to thank my supervisor Martin Doškář for being the wind beneath my academic wings. His guidance helps me move forward quickly. I am also grateful to Matěj Porubský for all his help and patience during the experimental verification of the results.

Abstract

Our study investigates the influence of geometrical parameters of two types of auxetic metamaterials on their effective properties. In particular, we focus on three-dimensional lattice structures, which we represent with discrete beam models of their respective Periodic Unit Cells (PUCs). Limiting the scope of the study to linear elasticity, we compute the effective response of PUCs by plugging the kinematic ansatz of the first-order numerical homogenisation into the strain energy expression arising from the Direct Stiffness Method and minimising the energy with respect to the periodic fluctuation field. The obtained effective stiffness matrices are post-processed to arrive at elastic parameters such as Poisson's ratios coefficients, which are reported in different directions with respect to the key geometrical parameters. The numerical study is validated against experiments on 3D printed samples loaded within a Thymos open-hardware test rig equipped with DIC-style optical measurements.

Keywords

auxetic metamaterial, first-order homogenisation, Periodic Unit Cell, effective Poisson's ratio

Contents

1 Introduction

Metamaterials are artificial materials with properties beyond those commonly found in nature. These properties are mainly determined by metamaterials' microstructure rather than by the chemical or physical parameters of their bulk constituents [1]. Due to technological advances in recent decades, complex microstructures of these metamaterials can be produced by manufacturing techniques such as 3D and even 4D printing [2], optical lithography [3], or electrospinning, which further increases the appeal of such materials. Mathematical modelling is then needed for efficient design of metamaterials, as it allows for circumventing lenghty experimental search for their optimal design.

Our study on the influence of geometry on the effective Poisson's ratio focuses on two variants (cubic and hexagonal) of a three-dimensional auxetic metamaterial proposed by Bückmann et al. [3] and shown in Fig. 1. Both designs exhibit a periodic microstructure allowing us to investigate only the response of a Periodic Unit Cell (PUC) as their Representative Volume Element (RVE).

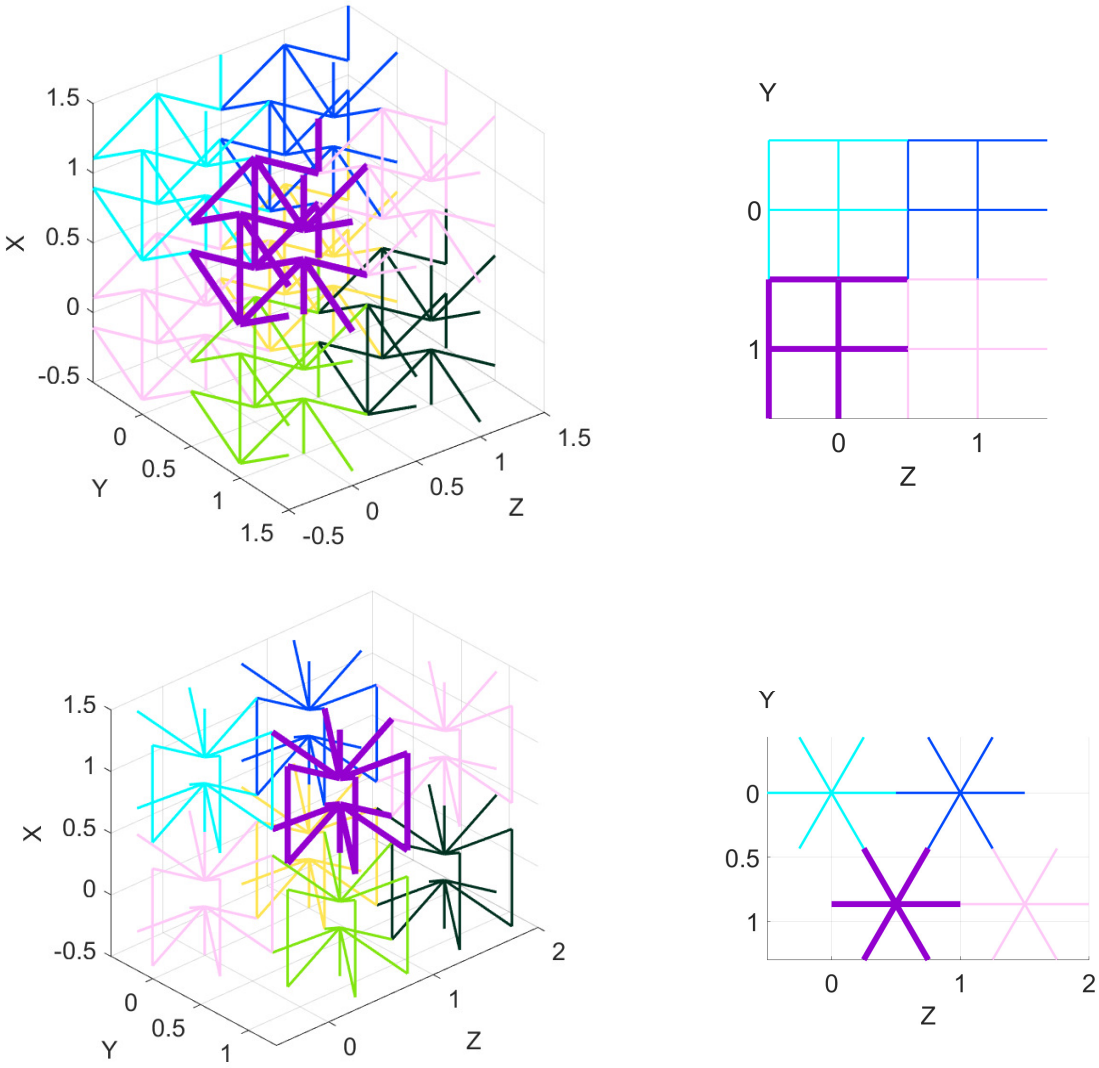

Figure 1: Two investigated auxetic metamaterials: a cubic variant (top) and a hexagonal variant (bottom). Insets on the right-hand side show a top view of the microstructures.

2 Geometry of the investigated metamaterials

The microstructure of the metamaterial is composed of several bow-tie structures, the geometry of which is controlled by the angle δ between the diagonal beam of the central bow-tie structure in the upper left quadrant and the yz plane passing through its initial node; see the insets on the right-hand side in Fig. 2. The 3D metamaterial is created by rotating the central bow-tie structure located in the xz plane around its vertical centre beams, as shown in Fig. 2. The cubic microstructure is obtained by rotation by 90°, which subsequently forms the central structure (dark blue). This central structure is complemented by a similar one (cyan), shifted by half a period in the yz plane. To create the PUC of the hexagonal variant, we perform 60° and 120° rotations of the bow-tie structure (purple). The height H of both PUCs will be considered as a single unit height.

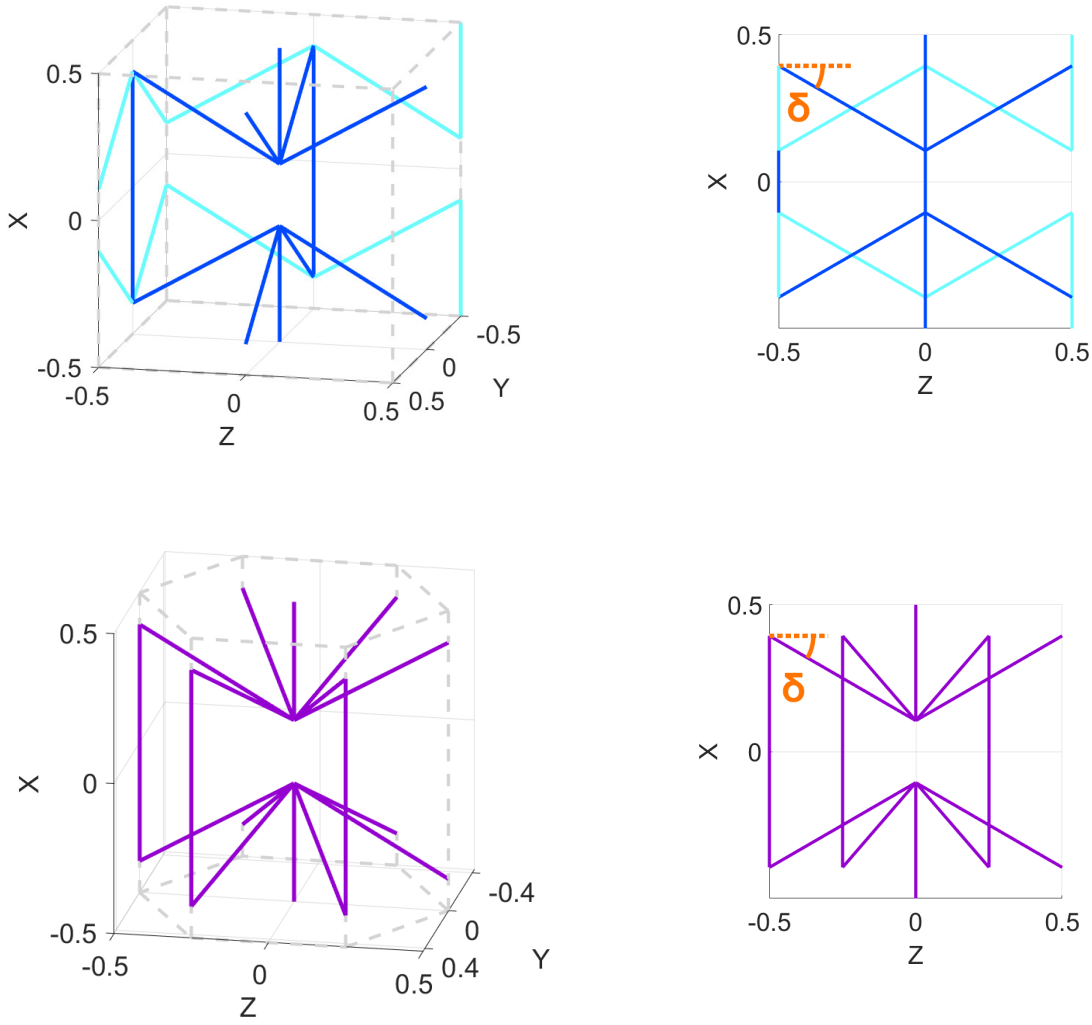

Figure 2: Periodic Unit Cells of cubic (top row) and regular hexagonal prismatic (bottom row) microstructure alongside their corresponding side views with highlighted angle δ, which controls the geometry of the metamaterial.

We model a PUC with discrete beams; we know the position of each node and the orientation of the beams that connect them. For this study, we assume a circular beam cross-section with diameter $d = 0.1H$. Consequently, cross-sectional characteristics follow as

$$\begin{aligned} A &= \frac{\pi}{4} \cdot d^2 \\ I &= \frac{\pi}{64} \cdot d^4 \\ J &= 2I = \frac{\pi}{32} \cdot d^4 \,, \end{aligned} \tag{1}$$

where A is the cross-section area, I is the second moment of inertia, and J is the polar moment of inertia. The volume of PUC is for the cubic variant $V_c = H^3$ and $V_h = \frac{3\sqrt{3}}{8} \cdot H^3$ for the hexagonal one.

3 Direct stiffness method

To compute a mechanical response of the PUC model, we use a linear discrete beam model that can be described by a linear relation

$$\mathsf{F} = \mathsf{K}\mathsf{u} \,, \tag{2}$$

where the vector F contains the forces and moments applied on all nodes, K is the stiffness matrix (assembled from individual submatrices K_i for each beam), and u is the displacement vector that successively contains subvectors of displacements u_i, v_i, w_i and rotations $\varphi_{x,i}$, $\varphi_{y,i}$, $\varphi_{z,i}$ of individual nodes i.

3.1 Local stiffness matrix

The local stiffness matrix K_i^l for the i-th beam follows from the Bernoulli-Euler beam theory [4] [5] and has size 12×12, due to the 6 unknowns located at the beginning (index b) and the end (index e) node of the beam. Individual parts that contribute to the stiffness matrix can be divided into 4 submatrices pertinent to:

1. membrane behaviour

$$\begin{bmatrix} X_b^l \\ X_e^l \end{bmatrix} = \frac{EA}{L_i} \begin{bmatrix} 1 & -1 \\ -1 & 1 \end{bmatrix} \begin{bmatrix} u_b^l \\ u_e^l \end{bmatrix}, \tag{3}$$

2. bending in xy plane

$$\begin{bmatrix} Y_b^l \\ M_{z,b}^l \\ Y_e^l \\ M_{z,e}^l \end{bmatrix} = \frac{2EI_z}{L_i} \begin{bmatrix} \frac{6}{L_i^2} & \frac{3}{L_i} & -\frac{6}{L_i^2} & \frac{3}{L_i} \\ \frac{3}{L_i} & 2 & -\frac{3}{L_i} & 1 \\ -\frac{6}{L_i^2} & -\frac{3}{L_i} & \frac{6}{L_i^2} & -\frac{3}{L_i} \\ \frac{3}{L_i} & 1 & -\frac{3}{L_i} & 2 \end{bmatrix} \begin{bmatrix} v_b^l \\ \varphi_{z,b}^l \\ v_e^l \\ \varphi_{z,e}^l \end{bmatrix}, \tag{4}$$

3. bending in xz plane

$$\begin{bmatrix} Z_b^l \\ M_{y,b}^l \\ Z_e^l \\ M_{y,e}^l \end{bmatrix} = \frac{2EI_y}{L_i} \begin{bmatrix} \frac{6}{L_i^2} & -\frac{3}{L_i} & -\frac{6}{L_i^2} & -\frac{3}{L_i} \\ -\frac{3}{L_i} & 2 & \frac{3}{L_i} & 1 \\ -\frac{6}{L_i^2} & \frac{3}{L_i} & \frac{6}{L_i^2} & \frac{3}{L_i} \\ -\frac{3}{L_i} & 1 & \frac{3}{L_i} & 2 \end{bmatrix} \begin{bmatrix} w_b^l \\ \varphi_{y,b}^l \\ w_e^l \\ \varphi_{y,e}^l \end{bmatrix}, \tag{5}$$

4. torsion

$$\begin{bmatrix} M^l_{x,b} \\ M^l_{x,e} \end{bmatrix} = \frac{GJ}{L_i} \begin{bmatrix} 1 & -1 \\ -1 & 1 \end{bmatrix} \begin{bmatrix} \varphi^l_{x,b} \\ \varphi^l_{x,e} \end{bmatrix}. \tag{6}$$

In the equations above, L_i refers to the length of a corresponding beam, E denotes Young's modulus, G stands for the shear modulus, and moments of inertia I_y, I_z are equal to I due to the circular cross-section of the beam. The local stiffness matrix K^l_i is obtained by combining the submatrices from Eqs. (3) - (6), each contributing to its specific degrees of freedom (DOFs).

3.2 Global stiffness matrix

The beams constituting the PUC's microstructure have different orientations. Hence, it is necessary to transform local displacements, rotations and end forces from Eqs. (3) - (6) into a global coordinate system. In our study, we adopted the approach of constructing a rotation matrix R_i for the i-th beam with Euler angles.

The beam's initial position is established by aligning its local coordinate system with the global one. Afterwards, we execute an extrinsic rotation around the global coordinate axes until the desired position is achieved. Rotation matrices

$$\mathsf{R}_x = \begin{bmatrix} 1 & 0 & 0 \\ 0 & \cos\alpha & -\sin\alpha \\ 0 & \sin\alpha & \cos\alpha \end{bmatrix}, \tag{7}$$

$$\mathsf{R}_y = \begin{bmatrix} \cos\beta & 0 & \sin\beta \\ 0 & 1 & 0 \\ -\sin\beta & 0 & \cos\beta \end{bmatrix}, \tag{8}$$

$$\mathsf{R}_z = \begin{bmatrix} \cos\gamma & -\sin\gamma & 0 \\ \sin\gamma & \cos\gamma & 0 \\ 0 & 0 & 1 \end{bmatrix}, \tag{9}$$

determine rotation around global x, y, z axes by angles α, β, γ, respectively, while each angle stands for rotation from the latest beam's position.

To obtain the rotation matrix R_i, we perform matrix multiplication

$$\mathsf{R}_i = \mathsf{R}_z \cdot \mathsf{R}_y \cdot \mathsf{R}_x, \tag{10}$$

where the sequence of the elements is based on the order in which the beam is rotated, starting with the rotation around the global x axis.

The nodal displacements and rotations are transformed at each end of the beam equally, so we can create a transformation matrix T_i by arranging the rotation matrix R_i on its diagonal.

$$\mathsf{T}_i = \begin{bmatrix} \mathsf{R_i} & 0 & 0 & 0 \\ 0 & \mathsf{R_i} & 0 & 0 \\ 0 & 0 & \mathsf{R_i} & 0 \\ 0 & 0 & 0 & \mathsf{R_i} \end{bmatrix} \tag{11}$$

The local stiffness matrix is then transformed into the global coordinate system using the relation

$$\mathsf{K}^g_i = \mathsf{T}^{\mathsf{T}}_i \mathsf{K}^l_i \mathsf{T}_i, \tag{12}$$

from which we obtain the global stiffness matrix K^g_i for each beam and localise them to the stiffness matrix K using Boolean localisation matrices L_i.

$$\mathsf{K} = \sum_i \mathsf{L}^{\mathsf{T}}_i \mathsf{K}^g_i \mathsf{L}_i \tag{13}$$

4 Homogenisation

The homogenisation process substitutes a heterogeneous PUC at the microscopic level with a corresponding macroscopic constitutive model, allowing us to study the effective behaviour of the PUC when treated as a material considering its microstructure. In our study, we are using the first-order numerical homogenisation to obtain the effective metamaterial properties.

4.1 Displacement decomposition

In the first-order homogenisation, the total displacement field $\vec{u}(\vec{x})$ is assumed in the form

$$\vec{u}(\vec{x}) = \vec{u}^{\,\mathbf{E}}(\vec{x}) + \vec{u}^{\,*}(\vec{x})\,, \tag{14}$$

where $\vec{u}^{\,\mathbf{E}}$ denotes the macroscopic and $\vec{u}^{*}$ is the fluctuation part of the displacement field caused by the heterogeneity of the metamaterial [6]. The macroscopic part $\vec{u}^{\,\mathbf{E}}$ of the displacement field corresponds to a situation under which an entire cell composed of homogeneous material would be subjected to a constant macroscopic strain tensor $\mathbf{E}$,

$$\mathbf{E} = \begin{bmatrix} E_{xx} & E_{xy} & E_{xz} \\ E_{yx} & E_{yy} & E_{yz} \\ E_{zx} & E_{zy} & E_{zz} \end{bmatrix}, \tag{15}$$

which results in a displacement field $\mathbf{u}^{\mathbf{E}}$ given as

$$\vec{u}^{\,\mathbf{E}}(\vec{x}) = \mathbf{E}\cdot\vec{x} = \begin{bmatrix} u^{\mathbf{E}} \\ v^{\mathbf{E}} \\ w^{\mathbf{E}} \end{bmatrix}. \tag{16}$$

For the first-order homogenisation, it is further assumed that the volumetric average of the gradient of the entire displacement field $\vec{u}(\vec{x})$ corresponds to the prescribed macroscopic deformation $\mathbf{E}$. By applying the symmetric gradient operator $\nabla^s = \frac{1}{2}(\nabla + \nabla^{\mathsf{T}})$ and averaging the result over a unit cell Ω, we obtain

$$\mathbf{E} = \frac{1}{|\Omega|}\int_\Omega \nabla^s\vec{u}(\vec{x})\,\mathrm{d}\vec{x} = \frac{1}{|\Omega|}\int_\Omega \nabla^s\vec{u}^{\,\mathbf{E}}(\vec{x}) + \nabla^s\vec{u}^{\,*}(\vec{x})\,\mathrm{d}\vec{x}\,, \tag{17}$$

where Ω represents the microscale domain of interest, being the metamaterial's macroscopic point [7].

The macroscopic part of the deformation $\vec{u}^{\,\mathbf{E}}(\vec{x})$ in Eq. (16) is defined such that

$$\mathbf{E} = \frac{1}{|\Omega|}\int_\Omega \nabla^s\vec{u}^{\,\mathbf{E}}(\vec{x})\mathrm{d}\vec{x}\,. \tag{18}$$

Consequently, the fluctuation part $\vec{u}^{\,*}(\vec{x})$ of the displacement field $\vec{u}(\vec{x})$, must have a zero volumetric average gradient, i.e.

$$\frac{1}{|\Omega|}\int_\Omega \nabla^s\vec{u}^{\,*}(\vec{x})\mathrm{d}\vec{x} = \mathsf{0}\,. \tag{19}$$

For our discrete beam model, Eq. (16) in a matrix form reads as

$$\mathsf{u}_i^{\mathsf{E}} = \begin{bmatrix} x_i & 0 & 0 & 0 & \frac{1}{2}z_i & \frac{1}{2}y_i \\ 0 & y_i & 0 & \frac{1}{2}z_i & 0 & \frac{1}{2}x_i \\ 0 & 0 & z_i & \frac{1}{2}y_i & \frac{1}{2}x_i & 0 \\ 0 & 0 & 0 & 0 & 0 & 0 \\ 0 & 0 & 0 & 0 & 0 & 0 \\ 0 & 0 & 0 & 0 & 0 & 0 \end{bmatrix} \mathsf{E} = \mathsf{Q}_i^{\mathsf{E}}\,\mathsf{E} \tag{20}$$

and couples nodal DOFs with the macroscopic deformation E, which is the vectorial representation of the symmetric second-order tensor $\mathbf{E}$, namely

$$\mathsf{E} = \begin{bmatrix} E_x & E_y & E_z & \Gamma_{yz} & \Gamma_{xz} & \Gamma_{xy} \end{bmatrix}^{\mathsf{T}} . \tag{21}$$

Now we can write the original degrees of freedom u depending on the macroscopic deformation E and the fluctuation unknowns u^*. Let's define the extended displacement vector

$$\widehat{\mathsf{u}} = \begin{bmatrix} \mathsf{E} \\ \mathsf{u}^* \end{bmatrix} , \tag{22}$$

then we can express degrees of freedom of our discrete beam model as

$$\mathsf{u} = \begin{bmatrix} \mathsf{Q}^E & \mathsf{I} \end{bmatrix} \begin{bmatrix} \mathsf{E} \\ \mathsf{u}^* \end{bmatrix} = \mathsf{Q}\,\widehat{\mathsf{u}} , \tag{23}$$

where I is the square identity matrix and Q^E is composed of the blocks $\mathsf{Q}_i^{\mathsf{E}}$ corresponding to the expression (20).

4.2 Periodic Boundary Conditions

To satisfy the constraint (19), we introduce Periodic Boundary Conditions (PBC), which is a natural model assumption for materials with periodic microstructures. Let's denote $\Pi(\vec{x})$ the mapping from the source part Γ^s of the boundary Γ onto its periodic image Γ^i. The fluctuation DOFs at a periodic point, denoted as $\mathsf{u}^*(\Pi(\vec{x}))$, are then equivalent to the corresponding DOFs $\mathsf{u}^*(\vec{x})$ at the boundary of the unit cell Γ^s

$$\mathsf{u}^*(\Pi(\vec{x})) = \mathsf{u}^*(\vec{x}) \quad \forall\, \vec{x} \in \Gamma^s . \tag{24}$$

To this end, we established a new vector a, containing unknown periodic fluctuation DOFs, which maps to u^* through the Boolean matrix P^*

$$\mathsf{u}^* = \mathsf{P}^*\,\mathsf{a} . \tag{25}$$

This step significantly reduces the number of unknowns in our equations.

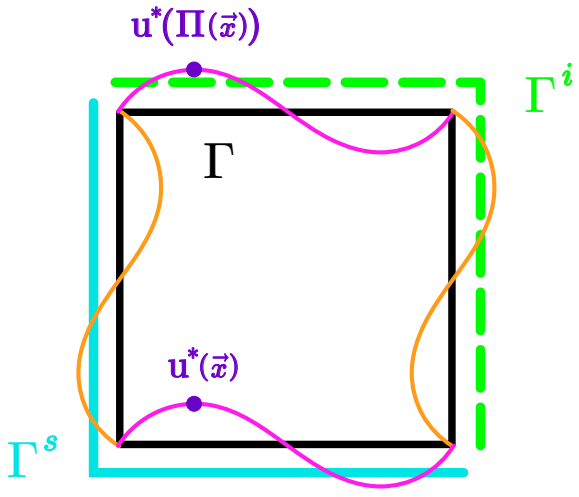

Figure 3: Illustration of Periodic Boundary Conditions for a 2D PUC. The fluctuation DOFs at periodic points $\mathsf{u}^*(\vec{x})$ at the source part Γ^s of the PUC boundary are equivalent to DOFs at it's periodic image Γ^i.

To prevent the PUC from moving as a rigid block during deformation, we prescribe zero fluctuation displacements at the node in the centre of the top edge of the PUC, illustrated with a black node in Fig. 4, while rotations remain free. Due to the periodicity, the fluctuation displacements must also vanish at the node in the centre of the bottom face of the PUC.

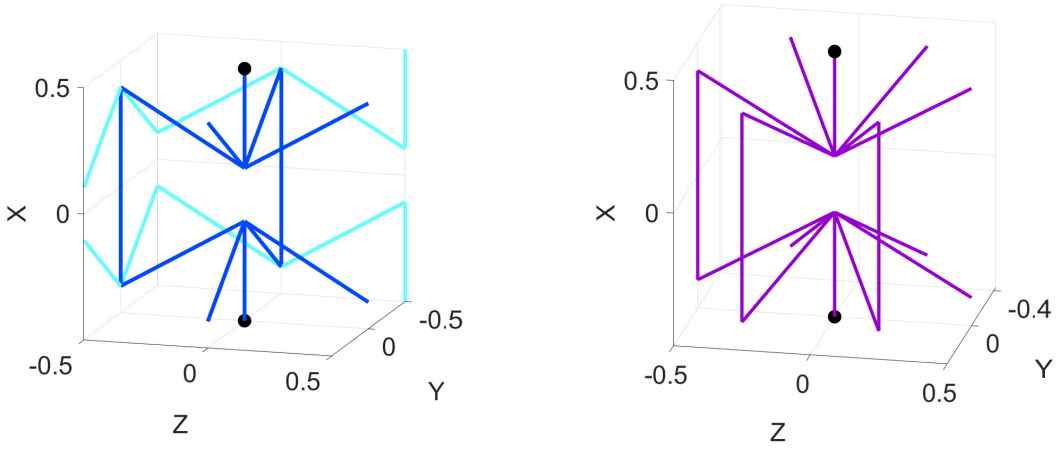

Figure 4: Fixed fluctuation displacements at nodes in the centre of the top and bottom face of the PUC, marked down with the black dots.

Similarly to Eq. (23), matrix $\widehat{\mathsf{P}}$ connects the macroscopic deformation E and the fluctuation unknowns a to the extended DOFs $\widehat{\mathsf{u}}$.

$$\widehat{\mathsf{u}} = \begin{bmatrix} \mathsf{E} \\ \mathsf{u}^* \end{bmatrix} = \begin{bmatrix} \mathsf{I} & \mathsf{P}^* \end{bmatrix} \begin{bmatrix} \mathsf{E} \\ \mathsf{a} \end{bmatrix} = \widehat{\mathsf{P}}\widehat{\mathsf{a}} \tag{26}$$

By connecting the macroscopic and fluctuation parts of the displacement field from Eq. (26) and considering Eq. (23) we get an expression for full-field displacement DOFs u based on unknown $\widehat{\mathsf{a}}$

$$\mathsf{u} = \mathsf{Q}\widehat{\mathsf{P}}\widehat{\mathsf{a}}\,. \tag{27}$$

4.3 Energy minimisation

For every macroscopic deformation E, there is a certain state into which the cell deforms, because it naturally attempts to reach the state with the lowest energy.

The energy $\mathcal{E}$ of a discrete beam model, which represents our PUC composed of beams and nodes, can be written as

$$\mathcal{E} = \frac{1}{2}\mathsf{u}^{\mathsf{T}}\mathsf{K}\mathsf{u}\,. \tag{28}$$

Similarly, for a linear elastic material of volume V that is subjected to a uniform deformation E at the macroscopic level, the relation for the energy can be expressed as

$$\mathcal{E}_M = V\frac{1}{2}\mathsf{E}^{\mathsf{T}}\mathsf{D}^{\mathrm{hom}}\mathsf{E}\,, \tag{29}$$

in which $\mathsf{D}^{\mathrm{hom}}$ is the material stiffness matrix of the desired homogenised metamaterial and vector E contains the individual macroscopic components of the deformation tensor in the vectorial form introduced in Eq. (21).

Plugging the unknowns from Eq. (27) into Eq. (28) yields an expression for PUC's energy based on macroscopic deformations E and fluctuation unknowns a

$$\mathcal{E}(\mathsf{E},\mathsf{a}) = \frac{1}{2}\begin{bmatrix}\mathsf{E}\\ \mathsf{a}\end{bmatrix}^{\mathsf{T}}\begin{bmatrix}\widehat{\mathsf{K}}_{\mathsf{EE}} & \widehat{\mathsf{K}}_{\mathsf{Ea}}\\ \widehat{\mathsf{K}}_{\mathsf{aE}} & \widehat{\mathsf{K}}_{\mathsf{aa}}\end{bmatrix}\begin{bmatrix}\mathsf{E}\\ \mathsf{a}\end{bmatrix} = \frac{1}{2}\,\widehat{\mathsf{a}}^{\mathsf{T}}\widehat{\mathsf{K}}\,\widehat{\mathsf{a}}, \tag{30}$$

where stiffness matrix $\widehat{\mathsf{K}}$ and its four submatrices $\widehat{\mathsf{K}}_{\mathsf{ij}}$ pertinent to E and a follow from

$$\widehat{\mathsf{K}} = \widehat{\mathsf{P}}^{\mathsf{T}}\mathsf{Q}^{\mathsf{T}}\mathsf{K}\,\mathsf{Q}\,\widehat{\mathsf{P}}\,. \tag{31}$$

Since we are interested in the response of the homogenised PUC to a prescribed macroscopic deformation E and not in displacement of its individual nodes, we express a with respect to the macroscopic deformation E of the cell. To this end, we keep the macroscopic deformation E fixed and determine the fluctuation displacements a as solution $\widetilde{\mathsf{a}}(\mathsf{E})$ that minimises energy $\mathcal{E}(\mathsf{E},\mathsf{a})$ for the given deformation E as

$$\widetilde{\mathsf{a}}(\mathsf{E}) = \underset{\mathsf{a}\in\mathbb{R}^n}{\operatorname{argmin}}\,\frac{1}{2}(\mathsf{E}^{\mathsf{T}}\widehat{\mathsf{K}}_{\mathsf{EE}}\mathsf{E} + \mathsf{E}^{\mathsf{T}}\widehat{\mathsf{K}}_{\mathsf{Ea}}\mathsf{a} + \mathsf{a}^{\mathsf{T}}\widehat{\mathsf{K}}_{\mathsf{aE}}\mathsf{E} + \mathsf{a}^{\mathsf{T}}\widehat{\mathsf{K}}_{\mathsf{aa}}\mathsf{a})\,, \tag{32}$$

where n represents the number of unknown fluctuation DOFs. As a result of the matrix $\widehat{\mathsf{K}}$ being both symmetric and positive definite, the quadratic form (30) attains the global minimum at the point of its zero gradient

$$\nabla_{\mathsf{a}}\mathcal{E}(\mathsf{E},\mathsf{a})\big|_{\mathsf{a}=\widetilde{\mathsf{a}}(\mathsf{E})} = \mathsf{K}_{\mathsf{aE}}\mathsf{E} + \mathsf{K}_{\mathsf{aa}}\widetilde{\mathsf{a}}(\mathsf{E}) = \mathsf{0}\,. \tag{33}$$

This provides us with the expression for the minimizer

$$\widetilde{\mathsf{a}}(\mathsf{E}) = -\mathsf{K}_{\mathsf{aa}}^{-1}\mathsf{K}_{\mathsf{aE}}\mathsf{E}\,. \tag{34}$$

Substituting the expression above into Eq. (30) yields an energy dependent entirely on the macroscopic deformations E,

$$\widetilde{\mathcal{E}}(\mathsf{E}) = \mathcal{E}(\mathsf{E},\widetilde{\mathsf{a}}(\mathsf{E})) = \frac{1}{2}\,\mathsf{E}^{\mathsf{T}}(\widehat{\mathsf{K}}_{\mathsf{EE}} - \widehat{\mathsf{K}}_{\mathsf{Ea}}\widehat{\mathsf{K}}_{\mathsf{aa}}^{-1}\widehat{\mathsf{K}}_{\mathsf{aE}})\;\mathsf{E} = \frac{1}{2}\,\mathsf{E}^{\mathsf{T}}\mathsf{K}^{\mathrm{eff}}\mathsf{E}\,. \tag{35}$$

Comparing the expression (35) with the formula for the energy of a homogeneous material of volume $V = |\Omega|$ subjected to a constant deformation E in Eq. (29), we arrive at the relation for the homogenised material stiffness of the auxetic metamaterial as

$$\mathsf{D}^{\mathrm{hom}} = \frac{1}{V}\mathsf{K}^{\mathrm{eff}}\,. \tag{36}$$

4.4 Effective Poisson's ratio

The procedure introduced in the previous sections yields the whole effective stiffness matrix. However, comparing and discussing the entire stiffness matrix is cumbersome. Here, we focus on the homogenised Poisson's effect as the primal objective of the auxetic metamaterial.

Because our structures are symmetric in three mutually perpendicular directions, we can expect the overall orthotropic response. Consequently, there are three different values of the Poisson's ratio depending on the direction of the prescribed relative deformation. Clearly, the Poisson's ratios ν in the xy and xz planes, ν_{xy} and ν_{xz}, will be the same due to the symmetry of PUC. Furthermore, ν_{yz} and ν_{zy} should be equal for the same reason.

We will refer to the stress in the metamaterial as Σ to distinguish the macroscopic level from the microscopic one. The stress-strain relation is linear because we work in the range of Hooke's law, so macroscopic stress can be written as

$$\mathsf{\Sigma} = \mathsf{D}^{\mathrm{hom}}\mathsf{E}\,, \tag{37}$$

which can be broken down into individual components as follows

$$\begin{bmatrix} \Sigma_x \\ \Sigma_y \\ \Sigma_z \\ \Sigma_{yz} \\ \Sigma_{xz} \\ \Sigma_{xy} \end{bmatrix} = \begin{bmatrix} D_{xx} & D_{xy} & D_{xz} & 0 & 0 & 0 \\ D_{yx} & D_{yy} & D_{yz} & 0 & 0 & 0 \\ D_{zx} & D_{zy} & D_{zz} & 0 & 0 & 0 \\ 0 & 0 & 0 & G_{yz} & 0 & 0 \\ 0 & 0 & 0 & 0 & G_{xz} & 0 \\ 0 & 0 & 0 & 0 & 0 & G_{xy} \end{bmatrix} \begin{bmatrix} E_x \\ E_y \\ E_z \\ \Gamma_{yz} \\ \Gamma_{xz} \\ \Gamma_{xy} \end{bmatrix}. \tag{38}$$

To determine the Poisson's ratio ν_{ij}, we perform a virtual uniaxial tension/compression experiment, in which we prescribe the macroscopic strain in the i-th direction and compute the strain in the j-th direction for the requirement of zero macroscopic stress in the j-th and k-th direction. This experiment results in the following relation

$$\widetilde{E}_j^{E_i} = \frac{D_{ik}D_{jk} - D_{ij}D_{kk}}{D_{jj}D_{kk} - D_{jk}^2} E_i\,. \tag{39}$$

Using (39) we can express Poisson's ratio for any direction, following its definition as a negative ratio of the derived and prescribed macroscopic strain. Consequently, the effective Poisson's ratio of an auxetic metamaterial is given by

$$\nu_{ij} = -\frac{\widetilde{E}_j^{E_i}}{E_i} = \frac{D_{ik}D_{jk} - D_{ij}D_{kk}}{D_{jk}^2 - D_{jj}D_{kk}}\,. \tag{40}$$

5 Numerical results

In this study, we investigated the range $\delta \in (0°, 45°)$ for the parametrisation of the two microstructural geometries (cubic and hexagonal); recall Figs. 1 and 2 from Section 2. This range was chosen to avoid beams' overlaps. The resulting values of the effective Poisson's ratios are plotted in Fig. 5. The numerical results comply with our assumptions of equal Poisson's ratio values in following directions:

$$\begin{aligned} \nu_{xy} &= \nu_{xz} \\ \nu_{yx} &= \nu_{zx} \\ \nu_{yz} &= \nu_{zy}\,, \end{aligned} \tag{41}$$

see also overlapping lines in Fig. 5. For the cubic PUC, we observed auxetic behaviour in the whole range of δ, while the metamaterial with hexagonal PUC exhibits pure auxetic properties only for angles $\delta \in \langle 10.56°, 45°)$. For the lower values of δ, the metamaterial is auxetic only in the xy and xz planes, with the highest Poisson's ratio value of $\nu_{yz} = 0.33$, which leads to the lateral contraction during stretching in the yz plane.

Poisson's ratios ν_{yx} and ν_{zx} are the one most influenced by the metamaterial's geometry and attain their minimum, within the investigated range of δ, from which their value starts increasing and slowly approaches remaining Poisson's ratios. Specifically, for the cubic PUC, the global minimum $\nu_{yx} = -1.98$ is achieved for $\delta = 13.78°$. The hexagonal PUC exhibits its minimal Poisson's ratio of

value $\nu_{yx} = -1.55$ at the angle $\delta = 15.92°$. The remaining pairs of Poisson's ratios, i.e. ν_{xy}, ν_{xz} and ν_{yz}, ν_{zy}, on the other hand, tend to decrease with the increasing angle δ across the entire range.

Additionally, we observe certain values of δ, at which selected Poisson's ratios coincide. In the cubic PUC, ν_{xy} and ν_{yz} attain the same value of -0.05 for $\delta = 3.32°$. The hexagonal PUC exhibits two such values of δ, $\delta = 16.96°$ and $\delta = 36.98°$, for which Poisson's ratios are equal to $\nu_{xy} = \nu_{yz} = -0.26$ and -0.63, respectively. In addition, the hexagonal PUC have equal Poisson's ratios ν_{xy} and ν_{yx} of value $\nu_{xy} = -0.82$ at the angle $\delta = 44.71°$.

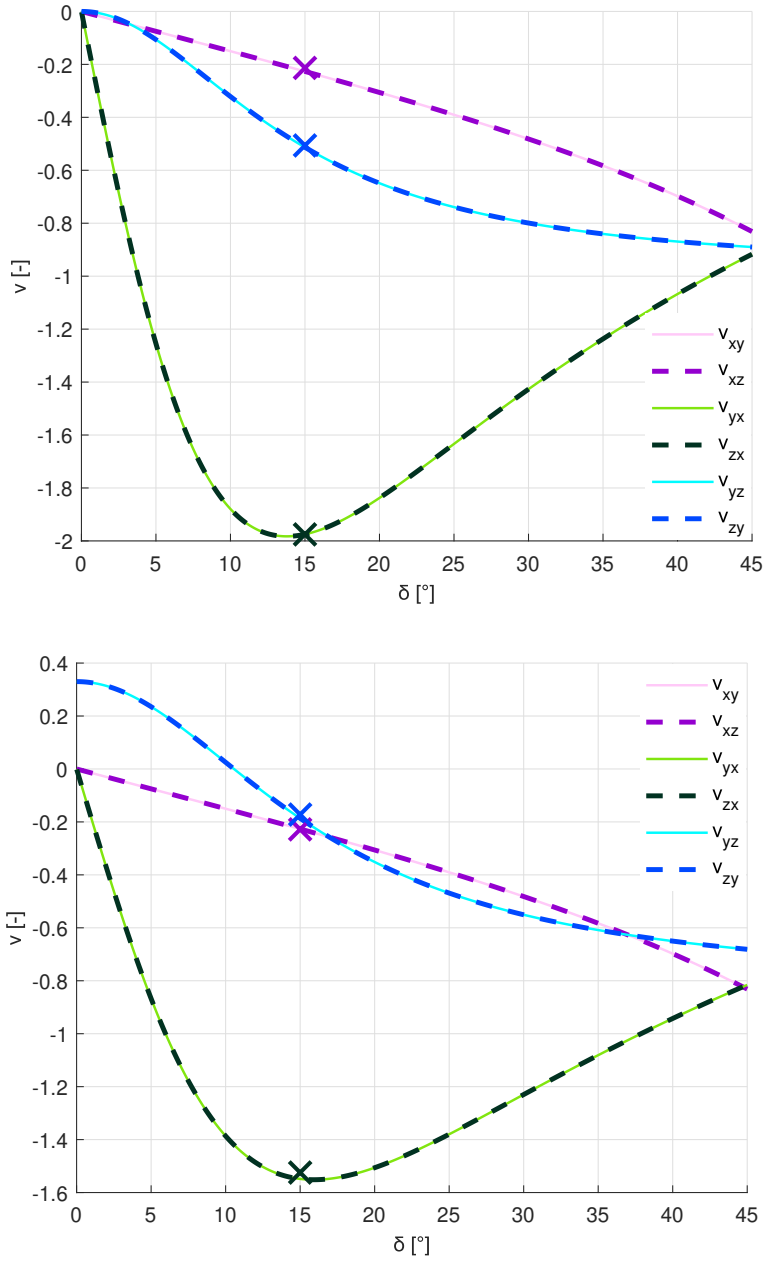

Figure 5: Poisson's ratio as a function of angle δ for cubic (top) and regular hexagonal prismatic (bottom) microstructure. The numerical results, illustrated by lines, are validated with experimental results marked with crosses for metamaterials with geometry at $\delta = 15°$.

6 Experimental section

We performed experiments to reinforce the validity of our numerical results. From each of the two microstructures, we created a 3D model based on the geometry corresponding to $\delta = 15°$, respecting the relations introduced in Section 2. The sample for the cubic microstructure is composed of 4×4×4 unit cells, which yields a total size of 5.0×5.0×5.0 cm. The sample for the hexagonal variant is constructed from 6×5×4 unit cells, resulting in a size of 5.5×5.3×4.3 cm.

6.1 3D print

3D models were produced with ELEGOO Mars Pro resin-based 3D printer. This type of printer uses a technique called stereolithography, which involves curing liquid resin layer by layer using an ultraviolet light source. For the resin mixture, we worked with two types of resin: tough and flex. The tough resin was Prusament Resin Tough Prusa and for flex one, we used PrimaCreator Value UV / DLP Resin FLEX. We experimented with various combinations of tough and flexible resins, ranging from a tough/flexible ratio of 60/40 to 100/0. Our goal was to find a mixture which is stiff enough to ensure that beams will remain straight (i.e. they do not buckle) during deformation but, at the same time, sufficiently flexible, such that beams do not break after a small compression. It turned out that the optimal choice is to use only the tough resin, which aligns the most with the behaviour of the numerical model.

After 3D printing, we cleaned the metamaterial from the liquid resin and removed the supports, which were necessary to print specific material sections, as the printer can only produce rigid material from the bottom to the top. The resulting 3D samples of the metamaterials are shown in Fig. 6.

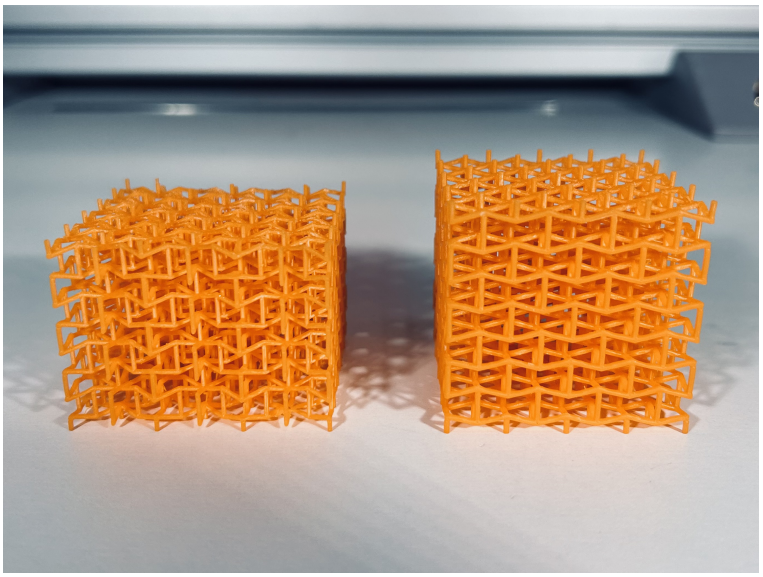

Figure 6: 3D printed metamaterials with hexagonal (left) and cubic (right) microstructure.

6.2 Experimental results

Using the open-hardware Thymos loading machine (shown in Fig. 7) controlled with a computer, we subjected the metamaterial sample to uniaxial compression. Each loading step involved a prescribed 0.2 mm vertical compression, which induced horizontal deformation due to Poisson's effect. Deformed state was captured by a DSLR camera, supplemented with two LED ligths to provide optimal lighting conditions. To reduced the friction between the loading plates and the tested sample and thus mimic the uniaxial compression, we applied a graphite powder to the surface between the sample and the loading machine. The lateral deformations of the tested sample were measured in AutoCAD software and then, along with the prescribed deformation, substituted into the formula for Poisson's ratio defined in Eq. (40), representing the negative ratio of derived (horizontal) and prescribed (vertical) deformation.

Our experimental results, depicted as crosses in Fig. 5, demonstrate a highly accurate alignment with the numerical results. To enhance clarity, we present here the average values from individual measurements of Poisson's ratio, since their differences were minimal and not distinctly visible in the resulting graph. Poisson's ratio values were determined within the deformation interval corresponding to the linear deformation assumptions of our numerical model. In this interval, no buckling of beams was observed and the overall response was linear.

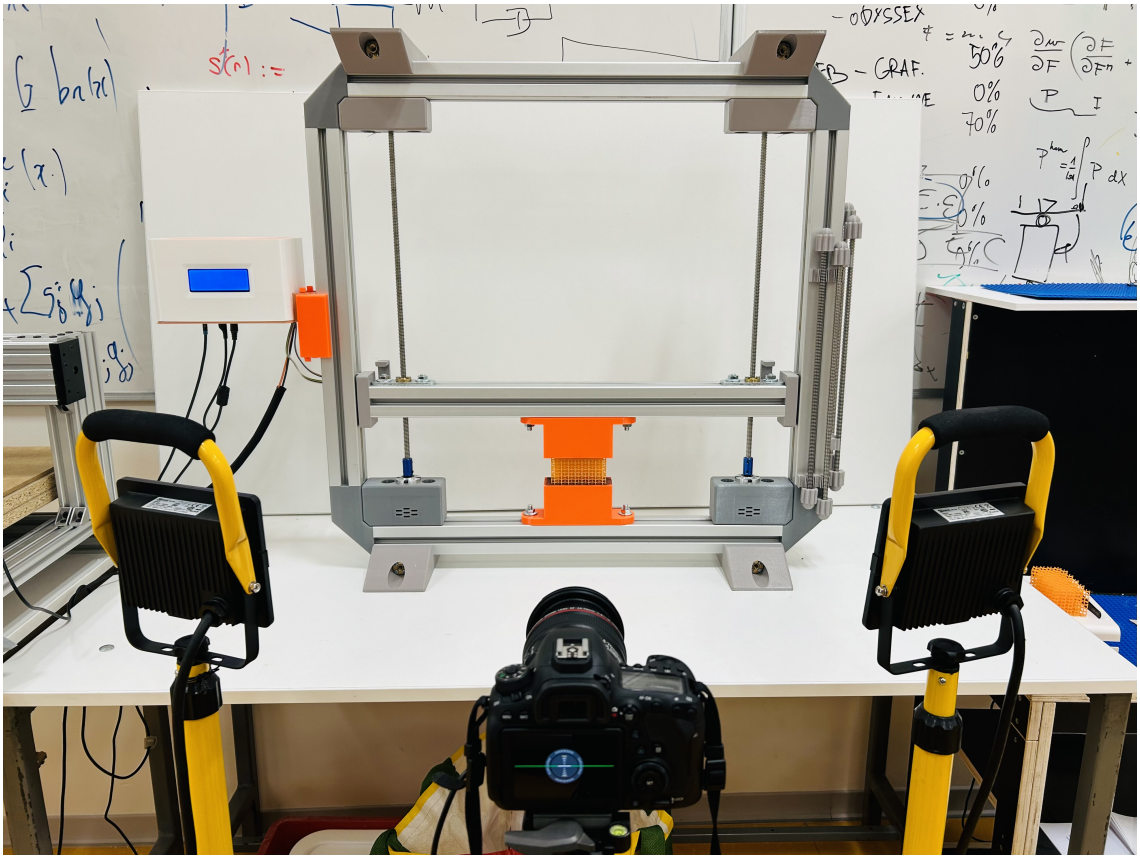

Figure 7: Loading system.

7 Summary

In this work, we investigated the influence of the geometry controlled by the angle δ in the bow-tie part of the microstructure on the effective Poisson's ratios of two three-dimensional metamaterials. Their PUCs were modelled with discrete beam elements, and the effective metamaterial properties were determined using Direct Stiffness Method and the first-order numerical homogenisation, resulting in a connection between their microstructure and macroscopic behaviour. Numerical results were validated against experiments performed on 3D printed samples loaded in a custom open-hardware test rig Thymos, showing a good agreement between experiments and numerical predictions.

Given the symmetries of both investigated microstructural geometries, we obtain three distinct values of Poisson's ratios as functions of angle δ. Two of these values decrease monotonically with increasing angle δ, while the remaining value (the same for ν_{yx} and ν_{zx}) exhibits a minimum within the studied range of ν. The cubic PUC features the minimum value $\nu_{yx} = -1.98$ for $\delta = 13.78°$, while the hexagonal PUC achieves the minimum value $\nu_{yx} = -1.55$ for $\delta = 15.92°$.

In conclusion, only the cubic PUC delivers auxetic behaviour in all directions for all investigated values of δ. The hexagonal PUC shares the same trait for $\delta \geq 10.56°$.

References

[1] E. Barchiesi, M. Spagnuolo, and L. Placidi, "Mechanical metamaterials: A state of the art," Mathematics and Mechanics of Solids, vol. 24, no. 1, pp. 212–234, Jan. 2019. DOI: 10.1177/1081286517735695.

[2] X. Zhou, L. Ren, Z. Song, et al., "Advances in 3D/4D printing of mechanical metamaterials: From manufacturing to applications," Composites Part B: Engineering, vol. 254, p. 110 585, Apr. 2023. DOI: 10.1016/j.compositesb.2023.110585.

[3] T. Bückmann, N. Stenger, M. Kadic, et al., "Tailored 3D Mechanical Metamaterials Made by Dip-in Direct-Laser-Writing Optical Lithography," Advanced Materials, vol. 24, no. 20, pp. 2710–2714, May 2012. DOI: 10.1002/adma.201200584.

[4] A. Kassimali, Matrix analysis of structures, 2nd ed. Australia ; Stamford, CT: Cengage Learning, 2012, ISBN: 978-1-111-42620-0.

[5] W. McGuire, R. H. Gallagher, and R. D. Ziemian, Matrix structural analysis, 2nd ed. New York: John Wiley, 2000, ISBN: 978-0-471-12918-9.

[6] J. Michel, H. Moulinec, and P. Suquet, "Effective properties of composite materials with periodic microstructure: A computational approach," Computer Methods in Applied Mechanics and Engineering, vol. 172, no. 1-4, pp. 109–143, Apr. 1999. DOI: 10.1016/S0045-7825(98)00227-8.

[7] M. Doškář and J. Novák, "A jigsaw puzzle framework for homogenization of high porosity foams," Computers & Structures, vol. 166, pp. 33–41, Apr. 2016. DOI: 10.1016/j.compstruc.2016.01.003.